EURASIP Journal on Applied Signal Processing 2004:16, 2492–2502

Speckle Reduction and Structure Enhancement by Multichannel Median Boosted Anisotropic Diffusion

Zhi Yang
Department of Electrical & Computer Engineering, University of Connecticut, Storrs, CT 06269-2157, USA
Email: yzhi@engr.uconn.edu

Martin D. Fox
Department of Electrical & Computer Engineering, University of Connecticut, Storrs, CT 06269-2157, USA
Email: fox@engr.uconn.edu

Received 31 August 2003; Revised 22 January 2004

We propose a new approach to reduce speckle noise and enhance structures in speckle-corrupted images. It utilizes a median-anisotropic diffusion compound scheme. The median-filter-based reaction term acts as a guided energy source to boost the structures in the image being processed. In addition, it regularizes the diffusion equation to ensure the existence and uniqueness of a solution. We also introduce a decimation and back reconstruction scheme to further enhance the processing result. Before the iteration of the diffusion process, the image is decimated and a subpixel shifted image set is formed. This allows a multichannel parallel diffusion iteration, and more importantly, the speckle noise is broken into impulsive or salt-pepper noise, which is easy to remove by median filtering. The advantage of the proposed technique is clear when it is compared to other diffusion algorithms and the well-known adaptive weighted median filtering (AWMF) scheme in both simulation and real medical ultrasound images.

Keywords and phrases: speckle noise, median filter, anisotropic diffusion, image decimation.

1. INTRODUCTION

In ultrasound, synthetic aperture radar (SAR), and coherent optical imaging, a major issue that is tackled is speckle. The presence of the speckle affects both human interpretation of the images and automated feature detection and extraction techniques. Much work has been done on speckle modeling and speckle reduction over the years. Most methods used in speckle reduction have focused on the use of the local mean, variance, median, and gradient.

Lee [1, 2] and Frost et al. [3] separately proposed their speckle reduction filters, which were adaptive to the local mean and variance. When local data are relatively homogeneous, a heavy filtering is applied because the local data only contain noise plus very slowly varying signal. On the other hand, when large variations exist in local data, a light filtering or no filtering is applied because this scenario is interpreted as an edge or other structural change. The problem with these filtering schemes is that they allow noisy edges to persist.

Loupas et al. [4] proposed an adaptive weighted median filter (AWMF) to reduce the speckle effect. Karaman et al. [5] proposed a region growth method and used a median filter within the grown regions to suppress speckle. Both [4, 5] applied a fixed-size filter window. Since there exists a particular root (see Section 2.2) for a given-size filter window [6, 7], the noise reduction ability of these adaptive filters is limited.

Hao et al. [8] used a multiscale nonlinear thresholding method to suppress speckle. They applied Loupas's AWMF to filter the image first, then put the filtered image and the difference image (obtained by subtracting the filtered image from the original image) into two wavelet decomposition channels. Each channel applied thresholding procedures for all decomposition scales. However, their method has only slightly better detail-preserving results and no significant improvement in speckle reduction over AWMF. This is because they used a global constant threshold in each scale. This threshold could not separate the speckle noise and the signal optimally.

Czerwinski et al. [9, 10] derived their approach using a generalized likelihood ratio test (GLRT). Local data are extracted along the different directions by a set of directional line-matched masks. For practical implementation reasons, they simplified the GLRT with white Gaussian

noise assumption (if the noise is not white, a prewhitening procedure is required) and used the local largest directional mean values to form the processed image. The theory of this method is well founded, but the practical implementation raises false alarms, such as false lines and edges. The processed result actually blurred the edges and produced artificial maximums (which could be misinterpreted as structures). Based on Czerwinski's scheme, Yang et al. [11] modified the directional line-matched masks to a set of directional line-cancellation masks to simulate the directional derivative process. After searching the local minimum directional derivative, they performed simple filtering (such as sample mean, median, etc.) along the direction of minimum directional derivative. This scheme took the coherent features of the structure and the incoherent features of the noise into account. Since the statistical variation along the direction is minimum, the processing result achieved significant structure enhancement while reducing the speckle. However, this method is weak in delineating sharp corners and has somewhat high computational cost.

Abd-Elmoniem et al. [12] proposed an anisotropic diffusion approach to perform speckle reduction and coherence enhancement. They applied an anisotropic diffusivity tensor into the diffusion equation to make the diffusion process more directionally selective. Although they generally had good results, the approach used raised the following questions. (1) It used isotropic Gaussian smoothing to regularize the ill-posed anisotropic diffusion equation. Although this kind of regularization has been proved to be able to provide existence, regularization, and uniqueness of a solution [13], it is against the anisotropic filtering principle. (2) The diffusivity tensor provided by a Gaussian smoothed image may not be effective for spatially correlated and heavy-tail distributed speckle noise. (3) Each speckle usually occupies several pixels in size. Without special treatment, there are chances to enhance the speckles, which is not desirable. Yu and Acton [14] proved that Lee [1, 2] and Frost's [3] filter schemes were closely related to diffusion processes, and adopted Lee's adaptive filtering idea into their anisotropic diffusion algorithm. However, the local statistics are actually isotropic, thus this method could not achieve the desired anisotropic processing.

In this paper, we will present a new anisotropic diffusion technique for speckle reduction and structure enhancement, which overcomes many of the problems mentioned above. The proposed technique is a compound technique. It utilizes the advantages of median filtering, anisotropic diffusion, and image decimation and reconstruction. The combination accelerates the iteration process and enhances the calculation efficiency. We applied the new method on artificial images, speckle-corrupted "peppers" image (this is a commonly used test image), and ultrasound medical images. The advantages of the proposed technique are clear when it is compared to other diffusion methods and the well-known AWMF method.

2. FOUNDATIONS FOR THE PROPOSED TECHNIQUE

2.1. Speckle model

The classical speckle model was proposed by Goodman [15, 16] for coherent optical imaging. According to this model, the signal in a detector element is a superposed result of a large number of incident subsignals. The magnitude of the signal usually follows a heavy-tailed distribution, typically Rayleigh. The speckles are spatially correlated. The correlation length is usually a few pixels (typically 3 to 5 pixels).

2.2. Median filter

The median filter is a well-known "edge preserving" nonlinear filter. It removes the extreme data while producing a smoothed output. The median filter is not a lowpass filter in the Fourier spectrum sense. Assuming the input data is an identical and independently distributed (i.i.d.) sequence, and the distribution is symmetrical, the median filter gives a similar result to the linear filter. If the distribution is *heavy tailed,* the median filtered result will be superior to the linear filtered result [6].

After repeated filtering with a given size mask, the median filtered result will reach a steady "state," referred to as the "root" image [6, 7]. Increasing the mask size will result in a smoother root image. On the other hand, once the root image has been reached with a larger size mask, decreasing the mask size will not change the root image. The root image should not be interpreted as noise free. It can contain larger scale noise. It is desirable to further filter the root image to provide additional cleaning, but it is not possible with a fixed-size median mask. It is not feasible to reach a new root image by increasing the mask size because valuable details can be removed by this approach.

2.3. Anisotropic diffusion

Diffusion is a fundamental physical process. For isotropic diffusion, the process can be modeled as a Gaussian smoothing with continuously increased variance. For anisotropic diffusion, the smoothing process becomes more directionally selective. Let $u(x, y, t)$ represent an image field with coordinates (x, y) at time t while D is the diffusion coefficient. The diffusion flux φ is defined as

$$\varphi = -D\nabla u. \tag{1}$$

With the matter continuity equation, we have

$$\frac{\partial u}{\partial t} = -\nabla \bullet \varphi. \tag{2}$$

Putting (1) and (2) together, we get the diffusion equation

$$\frac{\partial u}{\partial t} = \nabla \bullet (D\nabla u), \tag{3}$$

where "$\bullet$" represents the inner product of two vectors. When D is a constant, the diffusion process is isotropic. When D is a function of the directional parameters, the diffusion

process becomes anisotropic. If a source term $f(x, y, t)$ is added to the right-hand side of (3), the diffusion equation can be generalized to a nonhomogeneous partial differential equation

$$\frac{\partial u}{\partial t} = \nabla \bullet (D\nabla u) + \alpha f, \tag{4}$$

where α is a weighting coefficient.

To solve the above partial differential equation, the original image u_0 is used as the initial condition and the Neumann boundary condition is applied to the image borders:

$$\begin{aligned} u(x, y, t)_{t=0} &= u_0, \\ \partial_n u &= 0. \end{aligned} \tag{5}$$

The Neumann boundary condition avoids the energy loss in the image boundary during the diffusion process.

Perona and Malik (PM) [17] suggested two well-known diffusion coefficients:

$$D(s) = \frac{1}{1 + (s/k)^2}, \tag{6}$$

$$D(s) = \exp\left[-\left(\frac{s}{k}\right)^2 \right], \tag{7}$$

where $s = |\nabla u|$. With these diffusivity functions, the diffusion process will be encouraged when the magnitude of the local gradient is low, and restrained when the magnitude of the local gradient is high. The PM diffusion scheme is a nonlinear isotropic diffusion method according to Weickert [18]. However, as shown in Section 3.3, with two-dimensional explicit finite-difference implementation, D is a function of the direction, thus the diffusion process becomes anisotropic.

The parameter k is a threshold that controls when the diffusion is a forward process (smoothing) and when it is a backward process (enhancing edges). Both (6) and (7) give perceptually similar results, but (6) emphasizes noise removal while (7) emphasizes high-contrast preservation.

Catte et al. [13] pointed out that the PM approach has several serious practical and theoretical difficulties even though this method has worked very well with *ad hoc* treatments. These difficulties are centered around the existence, regularization, and uniqueness of a solution for (3) with diffusivity (6) or (7). Without special treatment, the PM method can misinterpret noises as edges and enhance them to create false edges.

Catte et al. changed $s = |\nabla u|$ in the PM diffusivity function to

$$s = |\nabla G_\sigma * u|. \tag{8}$$

Here G_σ is a Gaussian smoothing kernel and "$*$" is the convolution operator. In this approach, $|\nabla G_\sigma * u|$ is used to better estimate the local gradient instead of the noise sensitive $|\nabla u|$. They proved that this modification provides a sufficient condition for solution existence, regularization, and uniqueness.

However, the use of space-invariant isotropic Gaussian smoothing is contradictive to the anisotropic filtering principle, and Gaussian filtering tends to push the image structures away from their original locations. In the speckle reduction case, the diffusivity function calculated from the Gaussian smoothed image creates additional problems since the speckle noise is spatially correlated and heavy-tail distributed. For comparison purposes, the processing results with such *Gaussian regularized anisotropic diffusion* (GRAD) will be included in Section 4.

3. PROPOSED TECHNIQUE

3.1. Median boosted anisotropic diffusion technique

To perform anisotropic diffusion on speckle-corrupted images, a natural choice is replacing Gaussian smoothing by median filtering. The median filter is a smoothing operator, which is superior to Gaussian smoothing in the heavy-tail distributed speckle noise situation. Catte's proof concerning regularization (8) can still be applied to the median filtered case because the median filtered result is not worse than the Gaussian filtered result. Moreover, median filtering tends to preserve the image structure locations instead of dislocating them. As a result, the anisotropic diffusion process with median regularization provides better and more precise results.

We also propose to use a median filtered source term f in the homogeneous diffusion equation to form an interactive process, which combines both median filtering and natural diffusion. This technique is defined by the following relations:

$$\begin{aligned} \frac{\partial u}{\partial t} &= \nabla \bullet (D\nabla u) + \alpha f, \\ u(x, y, t)_{t=0} &= u_0, \\ \partial_n u &= 0, \end{aligned} \tag{9}$$

$$f = \text{median}(u), \tag{10}$$

where (6) holds and

$$s = |\nabla f|. \tag{11}$$

Speckle noise is signal-dependent noise. Typically, the bright regions have stronger noise than the dark regions. With the boosting term, the bright regions will be modified more heavily than the dark regions. The source term f provides two desirable effects. First, it provides a boosting force to guide (or normalize) the diffusion evolution. Like a "smart oven," it heats the image pixels with a progressively preset temperature field that is in favor of retaining image structures. Second, the source term will also accelerate the convergence rate compared to natural diffusion. On the other hand, since the diffusion process has different filtering mechanisms from the median filter, it will help to break the root barriers. The median filtered result will be progressively brought to a new root during the iterations. This interactive process will produce an image with less noise and enhanced structure. The constant α governs the interaction ratio. The use of α will be discussed more in Section 3.3.

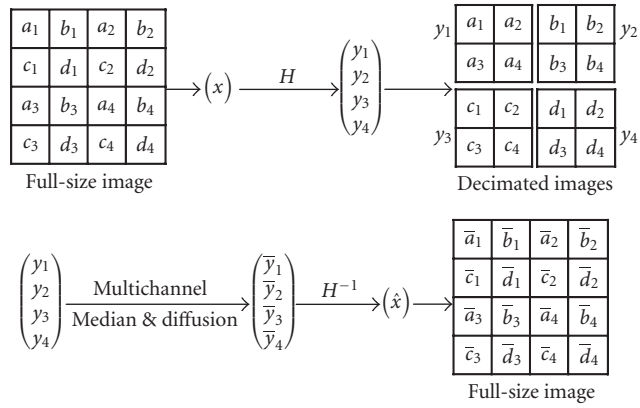

Figure 1: Illustration of the image decimation, multichannel median-diffusion, and full-image reconstruction. The decimation rate here is $\sqrt{p} = 2$.

3.2. Image decimation and multichannel processing

There are two apparent advantages to decimation of a speckle-corrupted image before further processing. First, decimation will break the speckles into quasi-impulsive or salt and pepper noise. The median filter has a well-known ability to deal with this type of noise. Second, decimation generates a set of subpixel shifted images. The size of these images is much smaller than the original image. The processing efficiency can be further improved by *square of the decimation rate* if parallel processing is applied.

The decimation process can produce aliasing in the decimated images, but the aliasing will not hurt the final reconstruction of the full-size image. Since we know exact subpixel shifts between the decimated images, the reconstruction process will be a well-posed super-resolution reconstruction process. The whole decimation and reconstruction processes can be formulated in the following manner:

$$\begin{aligned} y_1 &= H_1 x, \\ y_2 &= H_2 x, \\ &\vdots \\ y_i &= H_i x, \\ &\vdots \\ y_p &= H_p x \end{aligned} \tag{12}$$

or

$$Y = Hx, \tag{13}$$

and

$$Y = \begin{pmatrix} y_1 \\ y_2 \\ \vdots \\ y_p \end{pmatrix}, \qquad H = \begin{pmatrix} H_1 \\ H_2 \\ \vdots \\ H_p \end{pmatrix}, \tag{14}$$

where x is the original image denoted as a vector with length N^2, and $y_1, y_2, \ldots, y_p$ are the decimated images with different subpixel shifts. Each y_i is also denoted as a vector with length M^2, and $N = \sqrt{p} \times M$. Here, $\sqrt{p}$ is the decimation rate. $H_1, H_2, \ldots, H_p$ are the mapping matrices from x to different y_i's. They are $M^2 \times N^2$ sparse matrices.

Figure 1 illustrates the concept of the proposed decimation and multichannel processing technique. Assuming $\overline{y}_1$, $\overline{y}_2, \ldots, \overline{y}_p$ are the processed results of $y_1, y_2, \ldots, y_p$, there are many ways to estimate the full-size image [19]. In our approach, we used a direct interpolation method. Since a speckle usually occupies several pixels, the recommended decimation rate should typically be 2 or 3. We chose 2 for all examples in Section 4. High decimation rate can cause distortion or loss of image structures.

3.3. Explicit finite-difference approach

Following the PM explicit finite-difference approach, the proposed technique can be derived and numerically implemented using the following relations:

$$\begin{aligned} \frac{\partial u}{\partial t} &= \nabla \bullet (D \nabla u) + \alpha f, \\ \frac{u_{i,j}^{n+1} - u_{i,j}^{n}}{\tau} &= \frac{D_N(\nabla_N u_{i,j}^n / h) + D_S(\nabla_S u_{i,j}^n / h)}{h} \\ &\quad + \frac{D_E(\nabla_E u_{i,j}^n / h) + D_W(\nabla_W u_{i,j}^n / h)}{h} + \alpha f_{i,j}^n, \end{aligned} \tag{15}$$

where

$$\begin{aligned} \nabla_N u_{i,j}^n &= u_{i-1,j}^n - u_{i,j}^n, & \nabla_S u_{i,j}^n &= u_{i+1,j}^n - u_{i,j}^n, \\ \nabla_E u_{i,j}^n &= u_{i,j+1}^n - u_{i,j}^n, & \nabla_W u_{i,j}^n &= u_{i,j-1}^n - u_{i,j}^n. \end{aligned} \tag{16}$$

τ is the time interval between the consecutive iterations and h is the spatial distance of two neighboring pixels. $u_{i,j}^n$ refers to present pixel value at location (i, j) and $u_{i,j}^{n+1}$ is the next-time pixel value at the same location. N, S, E, W refer to north,

south, east, and west, respectively. The diffusion coefficients D_N, D_S, D_E, D_W are calculated from formulas (10), (6) with entries listed in (16), but replace the u's by the median filtered f's.

Parameter k in formula (6) is also calculated as k_N, k_S, k_E, k_W: they are set to the standard deviations of the corresponding difference value fields, represented by $\nabla_N u^n_{i,j}$, $\nabla_S u^n_{i,j}$, $\nabla_E u^n_{i,j}$, $\nabla_W u^n_{i,j}$. If a difference value at a particular location is smaller than the corresponding standard deviation, the difference value is considered to be induced by noise. If it is larger than the standard deviation, it is considered as an edge point or actual structural point, which should be preserved or enhanced during the process.

With the diffusion coefficients D_N, D_S, D_E, D_W, the diffusion process encourages smoothing along the direction where the pixel values are less changed and restrains smoothing in the direction where the pixel values are dramatically changed. Due to the discrete finite-difference implementation proposed above, the nonlinear diffusion process becomes anisotropic.

Let $h = 1$, then (15) becomes

$$u^{n+1}_{i,j} = u^n_{i,j} + \tau\left(D_N\nabla_N u^n_{i,j} + D_S\nabla_S u^n_{i,j} + D_E\nabla_E u^n_{i,j} + D_W\nabla_W u^n_{i,j}\right) + \tau\alpha f^n_{i,j}. \tag{17}$$

To assure the stability of the above iterative equation, τ should satisfy $0 \le \tau \le h^2/4$. Here, τ is set to 1/4. As a result,

$$u^{n+1}_{i,j} = u^n_{i,j} + \frac{D_N\nabla_N u^n_{i,j} + D_S\nabla_S u^n_{i,j} + D_E\nabla_E u^n_{i,j} + D_W\nabla_W u^n_{i,j}}{4} + \frac{\alpha}{4} f^n_{i,j}. \tag{18}$$

Let $\beta = \alpha/4$. To avoid processing bias, (18) can be modified to

$$u^{n+1}_{i,j} = (1-\beta)u^n_{i,j} + \frac{D_N\nabla_N u^n_{i,j} + D_S\nabla_S u^n_{i,j} + D_E\nabla_E u^n_{i,j} + D_W\nabla_W u^n_{i,j}}{4} + \beta f^n_{i,j}. \tag{19}$$

When $\beta = 0$, the above equation becomes a homogeneous median-regularized anisotropic diffusion (MRAD); when $\beta = 1$, the ongoing diffusion process is initialized to the median filtered result of the current image state (u^n). Choosing β too big results in heavy median filtering, which can smooth out the fine structures, while choosing β too small, the process would not realize the benefits of the median filtering. We chose $\beta = 0.2$ in our experiments. One thing should be mentioned here: the $\beta = 1$ case is similar to the median-diffusion method of Ling and Bovik [20] except they also used a median filtered u^n to calculate the difference values in (19).

Next, we want to talk about the stopping criteria for the iterations. Practically, the number of iterations can be decided by the mean square difference between the result of the previous iteration and the current iteration. When the value is less than a preset stopping criterion, the program stops iteration and produces a result. However, in the next section, the above stopping criterion was not used because to fairly compare different processing methods, one should use the same number of iterations in each case.

4. EXPERIMENTAL RESULTS

We generated an artificial image with the approximate speckle model

$$\omega = \omega_0 n, \tag{20}$$

where ω_0 is the noise-free image with gray level = 90 in bright regions and gray level = 50 in dark regions and n is the noise-only image, which is constructed by a running average of an i.i.d. Rayleigh distributed noise image with a 5×5 Gaussian mask with $\sigma = 2$. This simulates the correlation property of the speckle noise. ω is the observed signal. The image size is 380×318. Figure 2 shows the results of different filtering schemes on the artificial image. Specific information about the processing algorithms in Figure 2 is given in Table 1. Since the processing time for the image decimation (0.02 second) and the full-size image reconstruction (0.01 second) is negligible compared to the one-channel diffusion time (1.342 seconds), we only give the one-channel processing time in Tables 1, 3, 4, 5. Here, we use the short notation MGAD to represent the median boosted (or guided) and median regularized anisotropic diffusion and DMAD to represent the decimated median boosted and median regularized anisotropic diffusion.

Visually, the result processed by the new method is much sharper in terms of edge preservation and smoother in terms of speckle noise reduction than the other two filtered results. The execution time is also much shorter than the other two methods. For quantitative quality evaluation, we provide three metrics.

First, in terms of edge preserving or edge enhancement, we applied Pratt's figure of merit (FOM) to give a quantitative evaluation [21]. The FOM is defined by

$$\text{FOM} = \frac{1}{\max\{\hat{N}, N_{\text{ideal}}\}} \sum_{i=1}^{\hat{N}} \frac{1}{1 + d_i^2\lambda}, \tag{21}$$

where $\hat{N}$ and N_{ideal} are the numbers of detected and ideal edge pixels, respectively. d_i is the Euclidean distance between the ith detected edge pixel and the nearest ideal edge pixel. λ is a constant typically set to 1/9. The dynamic range of FOM is between $[0, 1]$. Higher value indicates better edge matching between processed image and the ideal image. We used the Laplacian of Gaussian (LOG) edge detector to find the edges in all processed results.

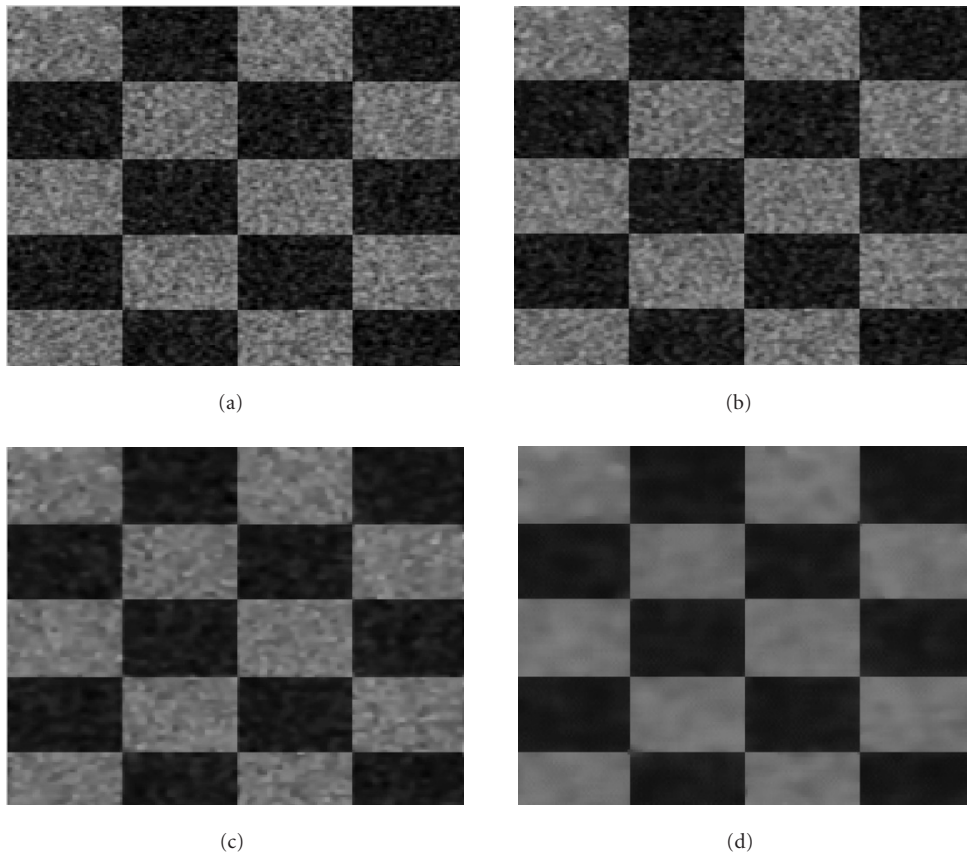

(a) (b) (c) (d)

Figure 2: (a) Artificial speckle image. (b) Processing result of the adaptive weighted median filter. (c) Processing result of the Gaussian regularized anisotropic diffusion. (d) Processing result of the decimated median boosted and median regularized anisotropic diffusion.

Table 1: Specific information about Figure 2.

	Figure 2b	Figure 2c	Figure 2d
Filter type	AWMF	GRAD	DMAD
No. of iterations	1	15	15
Mask size	3×3	Gaussian 3×3 $\sigma = 1$	Median 3×3
Execution time (s)	66.716	6.369	One channel 1.342
β	—	—	0.2

Second, the peak signal-to-noise ratio (PSNR) metric is also applied. PSNR evaluates the similarity between the processed image y and the ideal image x in terms of mean square error (MSE):

$$\text{PSNR} = 10 \times \log_{10}\left(\frac{g_{\max}^2}{\|x - y\|_2^2}\right), \tag{22}$$

where $g_{\max}$ is the upper-bound gray level of the image x or y (the images used throughout this paper are based on the scale of $[0, 255]$, so $g_{\max}$ is set to 255). $\| \bullet \|_2$ is an l_2-norm operator. Higher PSNR means a better match between the ideal and processed images.

Table 2: Processing result assessment for Figure 2.

Metrics	Filters		
	AWMF	GRAD	DMAD
FOM	0.3160	0.4806	0.8497
PSNR (dB)	21.8124	22.4398	22.9059
Q	0.1212	0.1266	0.1320

PSNR cannot distinguish the bias errors and random errors. In most cases, the bias errors are not as harmful as the random errors to the images, so we applied a third metric, the universal image quality index (Q), to evaluate the overall processing quality. This idea was proposed by Wang and Bovik [22]. The formula of the universal image quality index is

$$Q = \text{mean}\{Q_1 Q_2 Q_3\}, \tag{23}$$

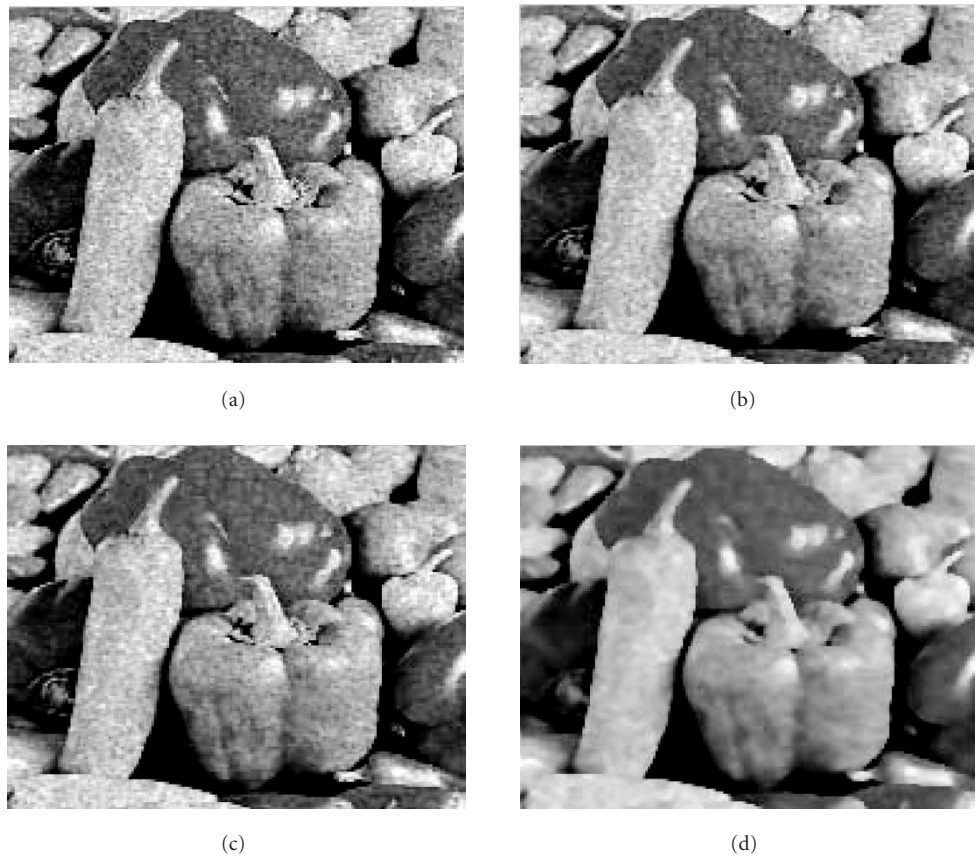

(a) (b)

(c) (d)

Figure 3: (a) Speckle-corrupted peppers image. (b) Processing result of the adaptive weighted median filter. (c) Processing result of the Gaussian regularized anisotropic diffusion. (d) Processing result of the decimated median boosted and regularized anisotropic diffusion.

Table 3: Specific information about Figure 3.

	Figure 3b	Figure 3c	Figure 3d
Filter type	AWMF	GRAD	DMAD
No. of iterations	1	4	4
Mask size	5×5	Gaussian 5×5 $\sigma = 2$	Median 5×5
Execution time (s)	257.491	4.687	One channel 1.502
β	—	—	0.2
PSNR (dB)	16.9141	16.8820	17.3466
Q	0.4300	0.4299	0.4947

where

$$Q_1 = \frac{\sigma_{xy}}{\sigma_x \sigma_y}, \qquad Q_2 = \frac{2 \cdot \overline{x}\,\overline{y}}{\overline{x}^2 + \overline{y}^2}, \qquad Q_3 = \frac{2 \cdot \sigma_x \sigma_y}{\sigma_x^2 + \sigma_y^2}. \quad (24)$$

Q_1 measures the local correlation (similarity) between images x and y, Q_2 measures the local processing bias, and Q_3 measures the local contrast distortion. The average value of $Q_1 Q_2 Q_3$ over the whole image gives the universal image quality index Q. The local measurement of each component of Q is based on an 8×8 sliding window throughout the whole image. Higher Q means a better match between the ideal and processed images.

Table 2 shows the evaluation results for the processed images in Figure 2. The FOM value indicates that the new method is better than other two methods in terms of edge preserving ability. PSNR and Q values indicate that the new method gives a better processing result in terms of MSE and the overall processing quality.

We also tested the proposed method on the peppers image (http://vision.ece.ucsb.edu/data_hiding/ETpeppers.html) (see Figure 3). The original image (512×512) is artificially corrupted by the speckle noise of model (20). The noisy image is shown in Figure 3a and the processed results of different filtering schemes are shown in Figures 3b, 3c, 3d. In this set of data, 5×5 filtering masks were used (this change will reduce the number of iterations; however, some finer details are lost compared to the 3×3 mask). In the example shown here, we obtained a rather good result with the new technique at the 4th iteration (with the least execution time; see Table 3).

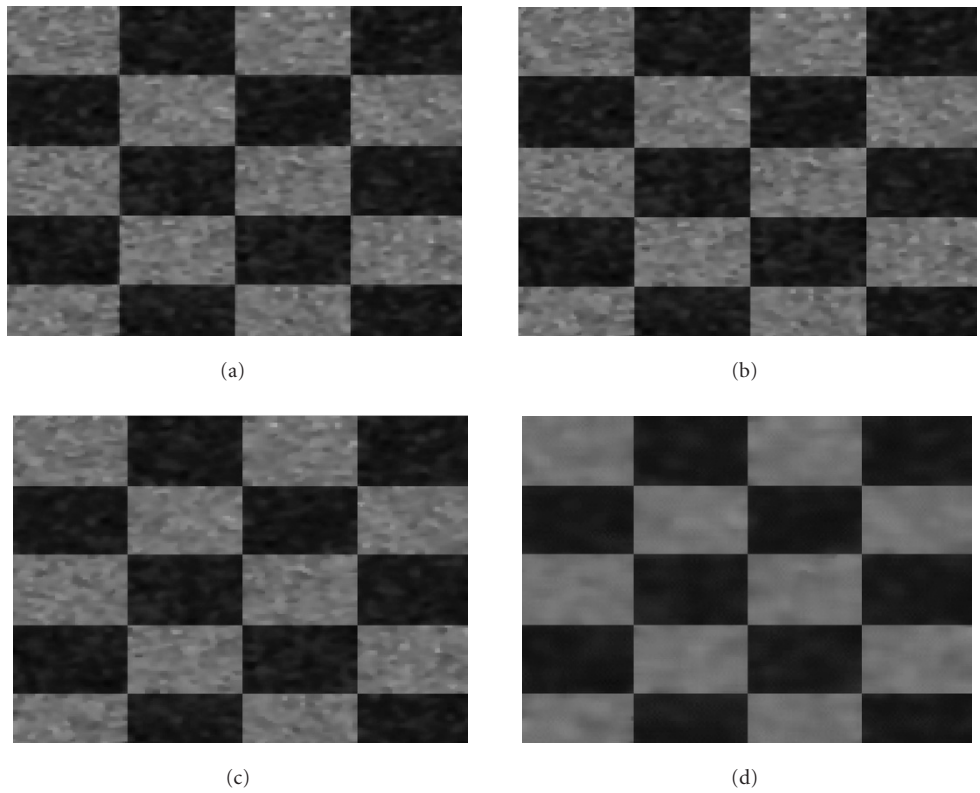

(a) (b) (c) (d)

Figure 4: (a) Processing result of the Gaussian regularized anisotropic diffusion. (b) Processing result of the median regularized anisotropic diffusion. (c) Processing result of the median guided and regularized anisotropic diffusion. (d) Processing result of the decimated median guided and regularized anisotropic diffusion.

Table 4: Specific information about Figure 4.

	Figure 4a	Figure 4b	Figure 4c	Figure 4d
Filter type	GRAD	MRAD	MGAD	DMAD
No. of iterations	15	15	15	15
Mask size	3×3	3×3	3×3	3×3
Execution time (s)	6.299	7.180	7.451	One channel 1.332
FOM	0.4896	0.5099	0.5559	0.8428
FOM improvement	—	4.13%	9.02%	51.61%
PSNR (dB)	22.4098	22.4409	22.5404	22.8881
PSNR improvement (dB)	—	0.0311	0.0995	0.3477
Q	0.1267	0.1279	0.1290	0.1323
Q improvement	—	0.95%	0.86%	2.56%

We did not perform the FOM evaluation for the peppers image since we did not have the ideal edge data. From Table 3, it is clear that the proposed method gives the best result, which is better than the AWMF by 0.4325 dB and the GRAD by 0.4646 dB in the PSNR and 15% in the Q metric.

In the new technique, there are three innovative components: median regularization, median boosting term (reaction term), and decimation. It is interesting to quantitatively assess to what degree each component contributes to the overall merit. The artificial image shown in Figure 2

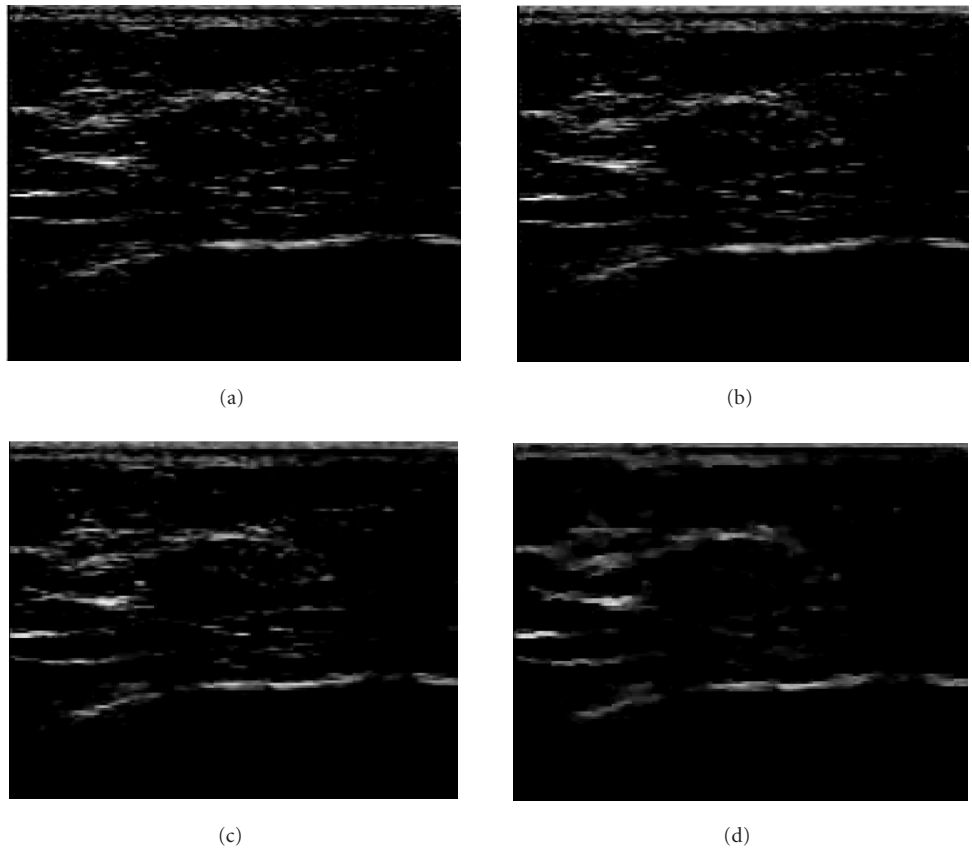

(a) (b) (c) (d)

Figure 5: (a) Ultrasound medical image. (b) Processing result of the adaptive weighted median filter. (c) Processing result of the Gaussian regularized anisotropic diffusion. (d) Processing result of the decimated median guided and regularized anisotropic diffusion.

Table 5: Specific information about Figure 5.

	Figure 5b	Figure 5c	Figure 5d
Filter type	AWMF	GRAD	DMAD
No. of iterations	1	6	6
Mask size	3×3	Gaussian 3×3 $\sigma=1$	Median 3×3
Execution time (s)	66.946	2.574	One channel 0.610
β	—	—	0.2

was used again to conduct the task because we have perfect knowledge about it. All the visual FOM, PSNR, and Q assessments can be performed. Figure 4 shows the results from the GRAD (Figure 4a) and the anisotropic diffusions while progressively adding the three components (Figure 4b—MRAD; Figure 4c—MGAD; Figure 4d—DMAD). There is no observable difference between Figures 4a and 4b, but heavy iterative test has shown that the result from GRAD starts to blur much earlier than the MRAD. Figure 4c appears smoother than Figures 4a, 4b. Figure 4d is the most enhanced result compared to the other three results in terms of background smoothness and edge sharpness. Table 4 provides the detailed filtering information and the quantitative assessing results. In terms of FOM criterion, the MRAD improves by about 4% over the GRAD, the MGAD improves by 9% over the MRAD, and the DMAD improves by almost 52% over the MGAD. In terms of PSNR criterion, the MRAD improves by 0.0311 dB over the GRAD, the MGAD improves by 0.0995 dB over the MRAD, and the DMAD improves by 0.3477 dB over the MGAD. In terms of Q criteria, the MRAD improves 0.95% over the GRAD, the MGAD improves 0.86% over the MRAD, and DMAD improves 2.56% over the MGAD. Although some improvements are small, they are consistent in all the experiments. From these numbers, we conclude that the decimation and parallel processing contribute the major gain. This test also verified that the median source term accelerated the convergence rate because with the same iteration numbers, the MGAD produced a better result than both GRAD and MRAD.

The proposed method was also tested on ultrasound medical images. Figure 5 shows the processing result compared with both the AWMF and GRAD methods. The size of the image is 380×318. Since we do not have the ideal image to perform the quantitative assessment, a subjective assessment has to be conducted. From Figure 5, it can be

seen that the proposed technique delineates the structures of the image better and suppresses the speckle most effectively. Table 5 provides the detailed filtering information.

5. DISCUSSION AND CONCLUSIONS

In this paper, we have proposed some important innovations to enhance the anisotropic diffusion technique. First, median regularization overcomes the shortcomings of Gaussian regularization. The modification provides optimal performance for the images corrupted by heavy-tail distributed speckle noise. Unlike the Gaussian regularization that tends to average the errors to every pixel in the filter window, the median filter drops the extreme data and preserves the most reasonable. Median filtering also preserves the edge locations. These desirable properties provide better diffusion coefficient estimation than Gaussian regularization. Second, although the median regularization is introduced to anisotropic diffusion and makes the diffusion more directionally selective, the diffusion process is still an average filter fundamentally. Adding median boosting term allows the process to take full advantage of the median filter. The interaction between the median boosting term and the anisotropic diffusion generates more desirable results than the single anisotropic diffusion filtering or median filtering. Third, and most importantly, the image decimation is used to break down speckle noise to quasi-impulse-type noise, which is easily removed by the median filter. Multichannel processing increases the processing speed greatly. Experimental results show that the new compound technique gives significant improvement in speckle reduction and image enhancement over previous techniques.

ACKNOWLEDGMENTS

The authors would like to thank the reviewers for their careful reading and constructive suggestions. The ultrasound medical image was collected under the funding support of NIH 9 R01 EB002136-2 and the study protocol was approved by the University of Connecticut Health (UConn) Center Institutional Review Board (IRB) Committee. Drs. Quing Zhu of ECE Department of UConn and Scott Kurtzman of UConn Health Center are thanked for providing the image.

REFERENCES

[1] J. S. Lee, "Digital image enhancement and noise filtering by use of local statistics," *IEEE Trans. on Pattern Analysis and Machine Intelligence*, vol. 2, no. 2, pp. 165–168, 1980.

[2] J. S. Lee, "Refined filtering of image noise using local statistics," *Computer Vision, Graphics, and Image Processing*, vol. 15, no. 2, pp. 380–389, 1981.

[3] V. S. Frost, J. A. Stiles, K. S. Shanmugan, and J. C. Holtzman, "A model for radar images and its application to adaptive digital filtering of multiplicative noise," *IEEE Trans. on Pattern Analysis and Machine Intelligence*, vol. 4, no. 2, pp. 157–166, 1982.

[4] T. Loupas, W. N. McDicken, and P. L. Allan, "An adaptive weighted median filter for speckle suppression in medical ultrasound images," *IEEE Trans. Circuits and Systems*, vol. 36, no. 1, pp. 129–135, 1989.

[5] M. Karaman, M. A. Kutay, and G. Bozdagi, "An adaptive speckle suppression filter for medical ultrasonic imaging," *IEEE Trans. on Medical Imaging*, vol. 14, no. 2, pp. 283–292, 1995.

[6] N. C. Gallagher and G. L. Wise, "Median filters: a tutorial," in *Proc. IEEE Int. Symp. Circuits and Systems (ISCAS 88)*, vol. 88, pp. 1737–1744, Espoo, Finland, June 1988.

[7] N. C. Gallagher and G. L. Wise, "A theoretical analysis of the properties of median filters," *IEEE Trans. Acoustics, Speech, and Signal Processing*, vol. 29, no. 6, pp. 1136–1141, 1981.

[8] X. Hao, S. Gao, and X. Gao, "A novel multiscale nonlinear thresholding method for ultrasonic speckle suppressing," *IEEE Trans. on Medical Imaging*, vol. 18, no. 9, pp. 787–794, 1999.

[9] R. N. Czerwinski, D. L. Jones, and W. D. O'Brien Jr., "Line and boundary detection in speckle images," *IEEE Trans. Image Processing*, vol. 7, no. 12, pp. 1700–1714, 1998.

[10] R. N. Czerwinski, D. L. Jones, and W. D. O'Brien Jr., "Detection of lines and boundaries in speckle images—application to medical ultrasound," *IEEE Trans. on Medical Imaging*, vol. 18, no. 2, pp. 126–136, 1999.

[11] Z. Yang, C. Li, J. Macione, and M. D. Fox, "Ultrasound B-scan image speckle noise reduction and boundary enhancement," in *Proc. 7th World Multi-Conference on Systemics, Cybernetics and Informatics*, vol. 4, pp. 258–263, Orlando, Fla, USA, July 2003.

[12] K. Z. Abd-Elmoniem, A. M. Youssef, and Y. M. Kadah, "Real-time speckle reduction and coherence enhancement in ultrasound imaging via nonlinear anisotropic diffusion," *IEEE Trans. on Biomedical Engineering*, vol. 49, no. 9, pp. 997–1014, 2002.

[13] F. Catte, P.-L. Lions, J.-M. Morel, and T. Coll, "Image selective smoothing and edge detection by nonlinear diffusion," *SIAM Journal on Numerical Analysis*, vol. 29, no. 1, pp. 182–193, 1992.

[14] Y. Yu and S. T. Acton, "Speckle reducing anisotropic diffusion," *IEEE Trans. Image Processing*, vol. 11, no. 11, pp. 1260–1270, 2002.

[15] J. W. Goodman, "Some fundamental properties of laser speckle," *Journal of the Optical Society of America*, vol. 66, no. 11, pp. 1145–1150, 1976.

[16] J. W. Goodman, "Statistical properties of laser speckle patterns," in *Laser Speckle and Related Phenomena*, Topics in Applied Physics, pp. 9–75, Springer-Verlag, Berlin, Germany, 1984.

[17] P. Perona and J. Malik, "Scale-space and edge detection using anisotropic diffusion," *IEEE Trans. on Pattern Analysis and Machine Intelligence*, vol. 12, no. 7, pp. 629–639, 1990.

[18] J. Weickert, "A review of nonlinear diffusion filtering," in *Scale-Space Theory in Computer Vision*, vol. 1252 of *Lecture Notes in Computer Science*, pp. 3–28, Springer-Verlag, Berlin, Germany, July 1997.

[19] S. C. Park, M. K. Park, and M. G. Kang, "Super-resolution image reconstruction: a technical overview," *IEEE Signal Processing Magazine*, vol. 20, no. 3, pp. 21–36, 2003.

[20] H. Ling and A. C. Bovik, "Smoothing low-SNR molecular images via anisotropic median-diffusion," *IEEE Trans. on Medical Imaging*, vol. 21, no. 4, pp. 377–384, 2002.

[21] W. K. Pratt, *Digital Image Processing*, Wiley, New York, NY, USA, 1978.

[22] Z. Wang and A. C. Bovik, "A universal image quality index," *IEEE Signal Processing Letters*, vol. 9, no. 3, pp. 81–84, 2002.

Zhi Yang received his B.S. degree from the Applied Physics Department, Northern Jiaotong University, Beijing, China, in 1990, and M.S. degree in electrical engineering from the China Academy of Railway Sciences (CARS), Beijing, China, in 1996. After graduation, he worked in CARS as a Research Engineer. He is currently a Ph.D. candidate in the Electrical & Computer Engineering Department, University of Connecticut. His research interests are in the areas of signal/image processing, medical imaging, and microprocessor-based embedded system.

Martin D. Fox received his B.E.E. degree from Cornell University in 1969, the Ph.D. degree from Duke University in 1972, and the M.D. degree from the School of Medicine, University of Miami, in 1983. His 1978 paper, "Multiple crossed beam ultrasound Doppler," received the Best Paper Award of the IEEE Transactions on Sonics and Ultrasonics for that year. He has published extensively in the areas of medical imaging and biomedical engineering. He has taught at the University of Connecticut since 1972, where he is presently a Full Professor of electrical and computer engineering. His research interests include ultrasound imaging and Doppler, microcontroller-based devices, biomedical instrumentation, and multidimensional image processing.